Editors' Suggestion

Interferometry of Non-Abelian Band Singularities and Euler Class Topology

Oliver Breach,[1,2] Robert-Jan Slager,[1] and F. Nur Ünal[1,*]
[1]TCM Group, Cavendish Laboratory, University of Cambridge, JJ Thomson Avenue, Cambridge CB3 0HE, United Kingdom
[2]Rudolf Peierls Centre for Theoretical Physics, Parks Road, Oxford OX1 3PU, United Kingdom

(Received 2 January 2024; accepted 1 August 2024; published 29 August 2024)

In systems with a real Bloch Hamiltonian band nodes can be characterized by a non-Abelian frame-rotation charge. The ability of these band nodes to annihilate pairwise is path dependent, since by braiding nodes in adjacent gaps the sign of their charges can be changed. Here, we theoretically construct and numerically confirm two concrete methods to experimentally probe these non-Abelian braiding processes and charges in ultracold atomic systems. We consider a coherent superposition of two bands that can be created by moving atoms through the band singularities at some angle in momentum space. Analyzing the dependency of excitations on the frame charges, we demonstrate an interferometry scheme passing through two band nodes, which reveals the relative frame charges and allows for measuring the multigap topological invariant. The second method relies on a single wave packet probing two nodes sequentially, where the frame charges can be determined from the band populations. Our results present a feasible avenue for measuring non-Abelian charges of band nodes and the direct experimental verification of braiding procedures, which can be applied in a variety of settings including the recently discovered anomalous non-Abelian phases arising under periodic driving.

DOI: 10.1103/PhysRevLett.133.093404

Introduction—Within the active field of topological insulators and semimetals [1–3], the role of on-site tenfold way symmetries, such as time reversal, particle-hole and chiral, as well as crystalline symmetries are by now rather uniformly understood in and out of equilibrium [4–16]. Recently there has been new progress in terms of multigap topological phases [17–21], where band subspaces (sets of isolated bands) can attain nontrivial invariants that do not *a priori* depend on the symmetry eigenvalues of the bands at high symmetry points and, hence, fall outside of all hitherto-known classifications [7–10]. When a system can be represented in terms of a real-valued Hamiltonian due to the presence of $\mathcal{C}_2\mathcal{T}$ or $\mathcal{PT}$ (twofold rotations or parity and time-reversal) symmetry, band degeneracies can carry non-Abelian frame charges [22]. The sign of these frame charges can be changed upon braiding band nodes in the momentum space, where the obstruction to annihilate the similarly valued charges is quantified by a multigap invariant, the Euler class [17–19]. Multigap considerations away from equilibrium have revealed even more exotic phenomena, such as novel quench signatures [23,24], optical responses [25–28], and anomalous non-Abelian phases that can exclusively arise under periodic driving [29].

Band nodes also play an important role in single-gap topological phases. Weyl nodes act as sources of Berry flux [30], while higher order degeneracies require stabilization of crystalline symmetries and are often associated with topological invariants. Individually, their properties can be probed in different experiments [31–36]. For example, the π-Berry flux of a Dirac cone has been measured through atomic momentum-space interferometry in optical lattices [32], and the winding of isolated linear or quadratic band touchings has been observed via exciting atoms by moving them through nodes [34]. Upon being elevated to multigap topologies, the hallmark gained by band singularities is non-Abelian frame charges that can induce a nontrivial Euler class. Consequently, a fundamental question arises whether there exists observable signatures of these non-Abelian charges, their braiding and this invariant.

We here address this question, providing an essential link to experiments. While frame charges correspond to $\pm\pi$ vortices *within* a gap, distinguishing them is difficult because it amounts to discriminating between zero and 2π phase windings of the frame after braiding. We demonstrate that these two cases impose certain constructive or destructive interference of atoms passing through different Euler nodes. Second, we construct another protocol for sequential excitation of atoms by moving them through two band nodes consecutively where the frame charges can be detected in the phase shift of resulting

*Contact author: fnu20@cam.ac.uk

oscillations in band populations. Our results reveal a physical manifestation of non-Abelian charges and their relative sign changes upon braiding in momentum space, imposing a feasible route to directly observe signatures of multigap band topology in experiments.

Non-Abelian frame charges and Euler class—For a real Hamiltonian, the eigenstates $|u_n(\boldsymbol{k})\rangle$ at quasimomentum $\boldsymbol{k}$ span an orthonormal triad or, in general, vielbein ("frame"): The space of spectralized Hamiltonians is given by $O(N)/O(1)^N = O(N)/\mathbb{Z}_2^N$ for $n \in N$ bands, where $N > 2$. The quotient ensures that flipping the signs of the eigenvectors does not change the Hamiltonian. Band singularities obstruct a unique assignment of the eigenstates and correspond to a π-rotation between the eigenstates that host the node [see Fig. 1(b)] [37]. Namely, the frame rotation (ϕ^{frame}) accumulates a π Berry phase upon circling around a node, where band singularities act as the analogs of π disclination vortices in biaxial nematics [38,39]. While within the two-band subspace (a single "gap") the nodes act as π rotations, we note that 2π rotations in fact correspond to -1 as $\pi_1[\mathrm{SO}(N)] = \mathbb{Z}_2$, accumulated frame charges *anticommute* with those in the adjacent gaps. Focusing on three bands, the frame charges associated with the nodes $\pi_1[\mathrm{SO}(3)/D_2] = Q$ take values in the quaternion group $Q = \{\pm 1, \pm i, \pm j, \pm k\}$ [38]. Consequently, braiding band nodes in momentum space (which can be achieved, e.g., using stress or strain [17,40], temperature effects [41], or periodic driving [29]), converts their charges and can ensure that a specific band subspace hosts similarly valued charges. In two dimensions, the resulting obstruction to annihilate these charges (nodes) between states n and $(n+1)$ is quantified by the Euler class [17,42],

$$\chi_{n,n+1}[\mathcal{D}] = \frac{1}{2\pi}\left[\int_{\mathcal{D}} \mathrm{Eu}\, dk_1 \wedge dk_2 - \oint_{\partial\mathcal{D}} \mathcal{A}\cdot d\boldsymbol{k}\right] \in \mathbb{Z}, \quad (1)$$

evaluated over any patch $\mathcal{D}$ encapsulating these nodes [Fig. 1(b)]. Here, we define the Euler form $\mathrm{Eu} = \langle \partial_{k_1} u_n(\boldsymbol{k}) | \partial_{k_2} u_{n+1}(\boldsymbol{k})\rangle - \langle \partial_{k_2} u_n(\boldsymbol{k}) | \partial_{k_1} u_{n+1}(\boldsymbol{k})\rangle$ and associated connection one-form, $\mathcal{A} = \langle u_n(\boldsymbol{k}) | \boldsymbol{\nabla} u_{n+1}(\boldsymbol{k})\rangle$.

The braiding and Euler class can effectively be captured by tracking Dirac strings (DSs) [29,42]. These are gauge objects connecting pairs of nodes in each gap (see Fig. 1) and represent the line across which the sign of the eigenstates change due to the π-Berry phase induced by the node. Hence, crossing a DS residing in an adjacent gap changes the sign of the frame charge, effectively encoding braiding rules of the band node charges [42].

Model—As a concrete example, we employ a $\mathcal{C}_2\mathcal{T}$-symmetric Kagome lattice, while our results apply to any system admitting an Euler description. The momentum-space Hamiltonian is written as

$$H(\boldsymbol{k}) = -2J\sum_{\beta\neq\beta'} \cos(\boldsymbol{k}\cdot\boldsymbol{d}_{\beta\beta'}) c_\beta^\dagger c_{\beta'} + \sum_\beta \Delta_\beta c_\beta^\dagger c_\beta, \quad (2)$$

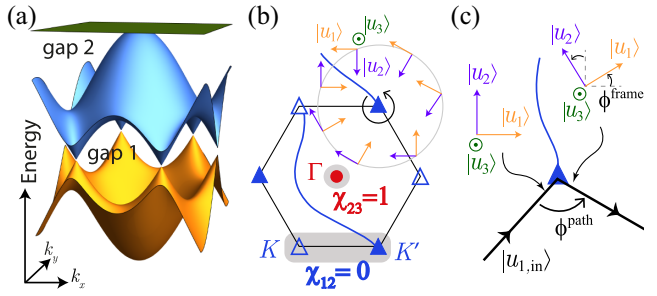

FIG. 1. (a) Kagome lattice band structure for $\Delta_\beta = 0$. (b) Linear band nodes (K, K') carry opposite non-Abelian frame charges ($\pm i \equiv \triangle/\blacktriangle$), and can annihilate ($\chi_{1,2} = 0$ in the shaded area). They act as $\pm\pi$ fluxes in gap 1, captured by the DS connecting them. Γ node is formed by two similar-valued frame charges ($+j \equiv \bullet$) that are obstructed to annihilate ($\chi_{2,3} = 1$). The orthonormal frame of the eigenstates (arrows) rotates around a band node, accumulating a π-phase jump at the DS. (c) A wave packet moving through a node at an angle ϕ^{path}, and finishing in a coherent superposition [Eq. (3)] due to the frame rotation by an angle ϕ^{frame}.

with nearest-neighbor hopping amplitudes J along the three directions $\boldsymbol{d}_{\beta\beta'}$ connecting three sublattices $\beta \in (A, B, C)$ and the annihilation (creation) operator $c_\beta^{(\dagger)}$ [29]. For vanishing sublattice offsets Δ_β, there are two linear band touching points which carry opposite frame charges [e.g., $\pm i$, depicted with empty and filled markers in Fig. 1(b)], hence a vanishing patch Euler class. The quadratic band touching point in gap 2 harbors $\chi = 1$, corresponding to two same-valued frame charges which we can assign to be $+j$ [51]. While quaternion frame charges act as $\pm\pi$ Berry fluxes in a given gap, conventional interferometry methods are insensitive to their signs and, hence, cannot *a priori* reveal the relative frame charges or their change after braiding.

Method 1: Interferometry—We employ a coherent superposition in the bands forming a singularity (i.e., the Euler subspace) to deduce the frame rotation around it relative to other nodes in this gap, hence, their relative frame charges. Consider moving a wave packet in momentum space in band 1 [$|u_{1,\text{in}}(\boldsymbol{k})\rangle$], which enters and exits a band node at some angle ϕ^{path} as in Fig. 1(c) [34]. Between the in-going and out-going paths the eigenstates frame is rotated by an angle ϕ^{frame}. Therefore, after passing through the band touching point, atoms are in a coherent superposition [42],

$$\begin{aligned} |u_{1,\text{in}}\rangle &\to |u_{1,\text{out}}\rangle\langle u_{1,\text{out}}|u_{1,\text{in}}\rangle + |u_{2,\text{out}}\rangle\langle u_{2,\text{out}}|u_{1,\text{in}}\rangle \\ &= \cos\phi^{\text{frame}}|u_{1,\text{out}}\rangle - \sin\phi^{\text{frame}}|u_{2,\text{out}}\rangle, \end{aligned} \quad (3)$$

given by the overlap with the final eigenstates $|u_{1,\text{out}}\rangle$ and $|u_{2,\text{out}}\rangle$, captured by the frame rotation ϕ^{frame}. Note that we here assume an adiabatic motion with respect to the third band, which can be generally satisfied due to the energetic

separation [Fig. 1(a)] and the orthonormality of the eigenstates. While the required path precision is within reach of state-of-the-art experiments [34], the desired superposition in the Euler subspace governed by ϕ^{frame} can be still created even if atoms might just miss the node realistically as we show in Supplemental Material [42]. For linear nodes, ϕ^{frame} winds always by π as ϕ^{path} winds by 2π. To demonstrate our scheme, we consider uniform and symmetric Hamiltonians (e.g., kagome) for a smooth winding $\phi^{\text{frame}} = \pm\phi^{\text{path}}/2$, while our methods readily apply to generic nodes [52].

When the system is characterized by an Euler class, the relative phase of the component excited into the second band depends on the chirality of the frame winding, i.e., the *full dreibein* that is naturally encoded by the Hamiltonian evolution. By analyzing two such excitations, we devise an interferometry of the Euler nodes to extract the relative non-Abelian frame charges and, hence, patch Euler class (1). We shall first present the idea in the simple setting of a kagome model by considering (K, K') nodes, where the $\mathcal{C}_6$ symmetry eliminates complicating effects of dynamic phases, isolating the key physics at play. We subsequently discuss more general settings, including effects of DSs and dynamic phases.

We consider a wave packet of a single spin state $|\uparrow\rangle$ localized in band $|u_1(\boldsymbol{k}_0)\rangle$, starting from $\boldsymbol{k}_0$ at equal distance to the targeted Euler nodes. Employing a $\pi/2$ pulse, a superposition of $(|\uparrow\rangle + |\downarrow\rangle)/\sqrt{2}$ can be created, where the pseudospin can be encoded by, e.g., hyperfine states [31,32]. As demonstrated in Fig. 2, we split the atoms such that $|\uparrow\rangle$ and $|\downarrow\rangle$ atoms follow symmetric paths I and II, passing through two nodes with angles ϕ^{path} and $-\phi^{\text{path}}$, respectively, before recombining. In optical lattices, this may be achieved by using a combination of an applied magnetic field gradient and lattice acceleration [31,32].

Assuming that the frame-rotation angle for the node I is ϕ^{frame}, the atoms following this path finish in the state $(c|u_1\rangle - s|u_2\rangle)|\uparrow\rangle$ as in Eq. (3), where $c \equiv \cos\phi^{\text{frame}}$ and $s \equiv \sin\phi^{\text{frame}}$ and the momentum index is suppressed for simplicity. If the node on path II carries the same charge with no DS in between, the frame features the same chirality on both nodes. However, since the path winds in the opposite direction ($-\phi^{\text{path}}$), the frame-rotation angle experienced on path II is $-\phi^{\text{frame}}$. Conversely, if the nodes have opposite charges, path II corresponds to a frame-rotation angle ϕ^{frame} [53].

Considering the paths together, the final state becomes

$$\frac{1}{\sqrt{2}}\left[(c|u_1\rangle - s|u_2\rangle)|\uparrow\rangle + (c|u_1\rangle \pm s|u_2\rangle)|\downarrow\rangle\right], \quad (4)$$

where $+(-)$ for down-spins on path II corresponds to same (opposite) charges. Applying another $\pi/2$ pulse before closing the interferometry then yields $c|u_1\rangle|\uparrow\rangle - s|u_2\rangle|\downarrow\rangle$ for similarly charged nodes, resulting in a mixture of both spin populations, $p_\uparrow = \cos^2(\phi^{\text{frame}})$ and $p_\downarrow = \sin^2(\phi^{\text{frame}})$. However, for oppositely charged nodes, the final state $c|u_1\rangle|\uparrow\rangle - s|u_2\rangle|\uparrow\rangle$ consists only of up spins $p_\uparrow = 1$. We demonstrate our interferometry technique along different paths in Figs. 2(a) and 2(b) with resulting populations given in Table I that are also numerically confirmed, where the relative non-Abelian frame charges are distinguished.

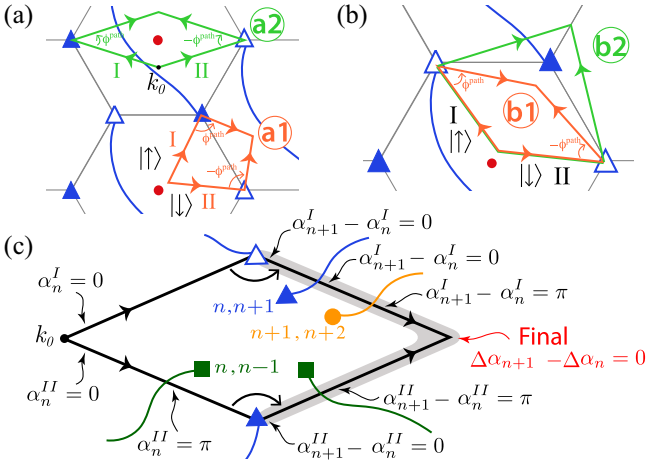

FIG. 2. (a),(b) Interferometry distinguishing relative frame charges of nodes in kagome lattice. Up- and down-spin atoms are moved along paths I and II, respectively, and recombined. Opposite (a) [same (b)] frame charges result in a single spin (mixture of both spins) as in Table I. In (b2), interferometry paths enclose an additional node, crossing a DS (blue line). (c) Illustration of the general interferometry (triangles, circles, and squares indicate nodes between different bands as labeled). Final geometric phases $\Delta\alpha_n - \Delta\alpha_{n+1} = 0$ indicate oppositely charged nodes, which annihilate if brought together within the shaded area, i.e., vanishing patch Euler class.

General configurations—Our interferometry technique readily caters to more complex band structures. The dynamic phases along the two paths considered above (Fig. 2) are equal under $\mathcal{C}_6$ symmetry and cancel in Table I (see Supplemental Material [42]). In general when targeted nodes are not at high-symmetry points, dynamic phases must be accounted for. This can be achieved, e.g., by measuring band energies along the interferometry with standard techniques like band mapping [31,54]. We present another method based on performing a reference interferometry loop with twice the acceleration in Supplemental Material [42].

Furthermore, there can be DSs traversed by the interferometry loop, which change the sign of the relevant eigenstates, leading to an additional π geometric phase. While the DS crossed twice in Fig. 2(a) yields no net effect as in Table I [55], the single crossing on path I in Fig. 2(b) induces a π phase shift between the spins and switches $p_\uparrow$ and $p_\downarrow$, but still entails a spin mixture for the similar-valued frame charges. We here give a proof for generic DS configurations that our interferometry scheme determines

TABLE I. Interferometry results for paths in Figs. 2(a) and 2(b). While opposite frame charges result in a single spin species, similar charges yield a mixture.

Paths	Final state	$p_\uparrow$	$p_\downarrow$	Charges
(a1)	$c\|u_1\rangle\|\uparrow\rangle - s\|u_2\rangle\|\uparrow\rangle$	1	0	Opposite
(a2)	$c\|u_1\rangle\|\uparrow\rangle - s\|u_2\rangle\|\uparrow\rangle$	1	0	Opposite
(b1)	$c\|u_1\rangle\|\uparrow\rangle - s\|u_2\rangle\|\downarrow\rangle$	$\cos^2\phi^{\text{path}}/2$	$\sin^2\phi^{\text{path}}/2$	Same
(b2)	$c\|u_1\rangle\|\downarrow\rangle - s\|u_2\rangle\|\uparrow\rangle$	$\sin^2\phi^{\text{path}}/2$	$\cos^2\phi^{\text{path}}/2$	Same

whether the nodes can annihilate if brought together along the paths closing the interferometry loop [Fig. 2(c)]. This reveals the relative frame charges and gauge-invariant Euler class (1) within this region.

We consider two Euler nodes between bands n and $n+1$, and focus on geometric phases $\alpha^{\text{I/II}}_{n(n+1)}$ in each band along paths I and II, where dynamic phases can be accounted for as before if required. We now analyze the effect of all possible DSs: (1) Right before the atoms starting in band n enter the nodes, the phase difference between the two paths $\Delta\alpha_n \equiv \alpha^{\text{II}}_n - \alpha^{\text{I}}_n$ can be 0 or π, depending on any DSs between the initial point and the nodes as depicted in Fig. 2(c). These have no effect as it will be carried over to the contributions in both bands on that path below [42]. (2) Just after exiting the nodes, the phase of the excited component $\alpha^{\text{I/II}}_{n+1}$ on the two arms depends on the frame charges, where we emphasize that the gauge is naturally fixed by the Hamiltonian evolution. If the charges are opposite as in Fig. 2(c), the total phase difference between the two paths are the same for both bands $\Delta\alpha_{n+1} - \Delta\alpha_n = 0$, while there will be a sign change $|\Delta\alpha_{n+1} - \Delta\alpha_n| = \pi$ for same charges. (3) When the wave packets are brought together avoiding other nodes, there can be three types of DSs crossed; within the Euler subspace and above or below gap, see Fig. 2(c): Crossing, e.g., the yellow DS changes $|u_{n+1}\rangle \to -|u_{n+1}\rangle$ on path I, which reflects on $\Delta\alpha_{n+1}$, as summarized in Table II for all cases. If the node itself is moved across the yellow DS, its frame charge flips. Indeed, we see that each time $\Delta\alpha_{n+1} - \Delta\alpha_n$ changes by π, the relative charge of the nodes changes. (4) The nodes' obstruction to annihilate within a region of the Brillouin zone is captured by the patch Euler class (1). We therefore conclude that the patch Euler class in the area enclosing the second half of the interferometry [i.e., postnode branches] vanishes $\chi_{n,n+1} = 0$ (is finite, $\chi_{n,n+1} = 1$) if $|\Delta\alpha_{n+1} - \Delta\alpha_n| = 0(\pi)$. Corresponding spin populations (after a $\pi/2$ pulse upon closing the interferometry [42]) are given in Table III, which are numerically verified.

We note that evaluating the Euler class is superfluous for two nodes separated by a reciprocal lattice vector. While we illustrate the relative charges using the simplest Kagome setting [Fig. 2], our scheme applies generically.

TABLE II. π-phase changes acquired by crossing possible DSs in Fig. 2(c) (shaded area) and corresponding effects on relative frame charges as explained in the text.

DS between bands	Effect on $\Delta\alpha_n$, $\Delta\alpha_{n+1}$	Relative charge
n and $n+1$	Both change by π	No change
n and $n-1$	$\Delta\alpha_n$ by π	Changes
$n+1$ and $n+2$	$\Delta\alpha_{n+1}$ by π	Changes

We validate this by employing a Kagome model with next-nearest-neighbor tunneling terms [20] which host several more singularities of various charges, see Supplemental Material [42]. Furthermore, under linear periodic driving, this model features an anomalous Euler phase [29] where the nontrivial patch invariant arises by virtue of a DS in the anomalous Floquet gap, which we confirm to be captured by our interferometry [42].

Method 2: Consecutive deflection—Our second method does not require an interferometry loop and offers the advantage of not increasing in complexity when symmetries are removed. This relies on a single wave packet entering and exiting the two targeted nodes [in the same way as in Eq. (3)] between bands $(n, n+1)$ consecutively [Fig. 3(a)]. Starting in band n, the final population p_n in this band depends on the frame-rotation angles $(\phi_1^{\text{frame}}, \phi_2^{\text{frame}})$, as well as the relative dynamic phase α' developed in between the nodes, which *a priori* complicates deducing the frame charges [56]. We circumvent this by expressing it after some algebra [42] as $p_n = [A\cos(2\phi_1^{\text{frame}} - \beta) + 1]/2$, where

$$A^2 = \cos^2(2\phi_2^{\text{frame}}) + \cos^2(\alpha')\sin^2(2\phi_2^{\text{frame}}), \tag{5}$$

$$\tan\beta = -\cos(\alpha')\tan(2\phi_2^{\text{frame}}). \tag{6}$$

The band population varies with ϕ_1^{frame} sinusoidally with an amplitude A and phase β. Crucially, the phase shift in Eq. (6) depends on whether the frame winds in the same or opposite direction around the second node (ϕ_2^{frame}), corresponding to same or opposite frame charges, provided that $\cos(\alpha')$ is known. The latter can be extracted from the amplitude (5), which reveals only $\cos^2(\alpha')$, by performing the experiment at double the acceleration to halve the dynamic phase.

TABLE III. Effects of possible phase changes (cf. Table II) on spin populations in bands n, $n+1$ after the interferometry: Relative frame charge depends only on $|\Delta\alpha_{n+1} - \Delta\alpha_n|$.

$\Delta\alpha_n$	$\Delta\alpha_{n+1}$	$p_\uparrow$	$p_\downarrow$	Charges
0	0	1	0	Opposite
π	π	0	1	Opposite
0	π	$\cos^2\phi^{\text{frame}}$	$\sin^2\phi^{\text{frame}}$	Same
π	0	$\sin^2\phi^{\text{frame}}$	$\cos^2\phi^{\text{frame}}$	Same

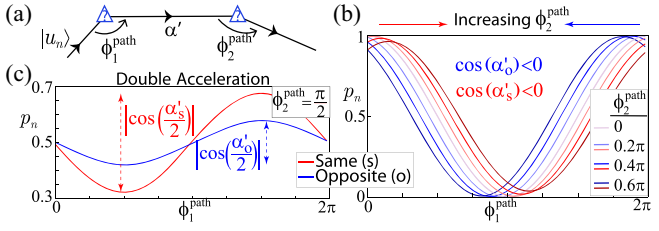

FIG. 3. (a) Illustration of the consecutive deflection method. Between the nodes, a relative dynamic phase α' is developed. (b) Starting from band $n = 1$, the final population p_1 oscillates as a function of ϕ_1^{path}. The phase-shift direction for increasing ϕ_2^{path} depends on the relative frame charge and sign of $\cos\alpha'$, here demonstrated in Kagome lattice for (K, K') nodes (2). (c) $\cos\alpha' < 0$ is deduced from Eq. (5) at double acceleration with $\phi_2^{\text{frame}} = \pi/4$.

Obtaining $\cos^2(\alpha'/2)$ thus yields $\cos\alpha' = 2\cos^2(\alpha'/2) - 1$. Alternatively, the dynamic phase can be directly calculated from energy measurements [31,54].

We numerically demonstrate this method by using the (K, K') nodes in Fig. 3 (see Supplemental Material [42] for more complicated settings), where $p_{n=1}$ oscillates as a function of the first turning angle $\phi_1^{\text{path}} = 2\phi_1^{\text{frame}}$. Repeating for different turning angles in node 2 induces a phase shift, direction of which reveals the relative frame charges. Figure 3(c) reveals $\cos\alpha' < 0$ in both cases, and therefore the phase (β) increases (decreases) for similar (opposite) frame charges.

Discussion—Our two interferometric schemes for extracting non-Abelian frame charges of real Hamiltonians require control on lattice acceleration and path precision that have been already demonstrated in ultracold atom experiments [32,34]. While the first method involves two measurements—the actual interferometry and in general a reference loop if dynamic phases differ along each path [42]—the second method relies on several measurements for a range of $\phi_{1,2}^{\text{path}}$ values to detect the phase shift but applies independently of underlying lattice symmetries. We note that pseudospins in Method 1 can be employed for guiding atoms along an interferometry loop [32] and further combining with band specific readouts of atoms reveals individual terms in Table I. Method 2 can be fine-tuned for a specific experiment as well. For example, for known frame windings around individual nodes (e.g., uniform under C_6 symmetry [42]), one requires only three measurements: Two for observing p_n under double acceleration by choosing $|\phi_1^{\text{frame}}| = |\phi_2^{\text{frame}}| = \pi/4$ and reversing the sign of ϕ_1^{frame}, which yield $\sin^2(\alpha'/4)$ and $1 - \sin^2(\alpha'/4)$ to find $\cos^2(\alpha'/2)$. Repeating the first measurement at normal acceleration then discloses $1 - \cos^2(\alpha'/2)[\cos^2(\alpha'/2)]$ for similar [opposite] charges. We further demonstrate our techniques' robustness under experimental imperfections in [42], putting them within reach of state-of-the-art experiments [32,34].

The interferometry and consecutive deflection methods reveal the relative frame charge along the path joining the nodes. Hence, by varying the route connecting the nodes, our techniques pave the way for directly demonstrating the non-Abelian and path dependent nature of braiding in experiments. Given the essential role of such charges in constituting Euler class [17–19], these serve as a crucial route towards experimentally probing multigap topologies in and out of equilibrium [29].

Acknowledgments—O. B. thanks James Walkling and Calvin Hooper for productive discussions. We acknowledge discussions with Dan Stamper-Kurn and Adrien Bouhon. O. B. acknowledges funding from the Clarendon Fund, Merton College, and the Leverhulme Trust. R.-J. S. acknowledges funding from a New Investigator Award, EPSRC Grant No. EP/W00187X/1, a EPSRC ERC underwrite Grant No. EP/X025829/1, and a Royal Society exchange Grant No. IES/R1/221060 as well as Trinity College, Cambridge. F. N. Ü. acknowledges funding from the Marie Skłodowska-Curie programme of the European Commission Grant No. 893915, Simons Investigator Award [Grant No. 511029], Trinity College Cambridge, and thanks the Aspen Center for Physics for their hospitality, where this work was partially funded by a grant from the Sloan Foundation.

[1] X.-L. Qi and S.-C. Zhang, Topological insulators and superconductors, Rev. Mod. Phys. **83**, 1057 (2011).
[2] M. Z. Hasan and C. L. Kane, Colloquium: Topological insulators, Rev. Mod. Phys. **82**, 3045 (2010).
[3] N. P. Armitage, E. J. Mele, and A. Vishwanath, Weyl and Dirac semimetals in three-dimensional solids, Rev. Mod. Phys. **90**, 015001 (2018).
[4] L. Fu, Topological crystalline insulators, Phys. Rev. Lett. **106**, 106802 (2011).
[5] R.-J. Slager, A. Mesaros, V. Juričić, and J. Zaanen, The space group classification of topological band-insulators, Nat. Phys. **9**, 98 (2012).
[6] C.-K. Chiu, J. C. Y. Teo, A. P. Schnyder, and S. Ryu, Classification of topological quantum matter with symmetries, Rev. Mod. Phys. **88**, 035005 (2016).
[7] J. Kruthoff, J. de Boer, J. van Wezel, C. L. Kane, and R.-J. Slager, Topological classification of crystalline insulators through band structure combinatorics, Phys. Rev. X **7**, 041069 (2017).
[8] H. C. Po, A. Vishwanath, and H. Watanabe, Symmetry-based indicators of band topology in the 230 space groups, Nat. Commun. **8**, 50 (2017).
[9] B. Bradlyn, L. Elcoro, J. Cano, M. G. Vergniory, Z. Wang, C. Felser, M. I. Aroyo, and B. A. Bernevig, Topological quantum chemistry, Nature (London) **547**, 298 (2017).
[10] A. Kitaev, Periodic table for topological insulators and superconductors, AIP Conf. Proc. **1134**, 22 (2009).
[11] A. Bouhon, A. M. Black-Schaffer, and R.-J. Slager, Wilson loop approach to fragile topology of split elementary band

representations and topological crystalline insulators with time-reversal symmetry, Phys. Rev. B **100**, 195135 (2019).
[12] H. C. Po, H. Watanabe, and A. Vishwanath, Fragile topology and Wannier obstructions, Phys. Rev. Lett. **121**, 126402 (2018).
[13] R. Roy and F. Harper, Periodic table for Floquet topological insulators, Phys. Rev. B **96**, 155118 (2017).
[14] M. S. Rudner, N. H. Lindner, E. Berg, and M. Levin, Anomalous edge states and the bulk-edge correspondence for periodically driven two-dimensional systems, Phys. Rev. X **3**, 031005 (2013).
[15] T. Kitagawa, E. Berg, M. Rudner, and E. Demler, Topological characterization of periodically driven quantum systems, Phys. Rev. B **82**, 235114 (2010).
[16] S. Lieu, M. McGinley, and N. R. Cooper, Tenfold way for quadratic Lindbladians, Phys. Rev. Lett. **124**, 040401 (2020).
[17] A. Bouhon, Q. Wu, R.-J. Slager, H. Weng, O. V. Yazyev, and T. Bzdušek, Non-Abelian reciprocal braiding of Weyl points and its manifestation in ZrTe, Nat. Phys. **16**, 1137 (2020).
[18] J. Ahn, S. Park, and B.-J. Yang, Failure of Nielsen-Ninomiya theorem and fragile topology in two-dimensional systems with space-time inversion symmetry: Application to twisted bilayer graphene at magic angle, Phys. Rev. X **9**, 021013 (2019).
[19] A. Bouhon, T. Bzdusek, and R.-J. Slager, Geometric approach to fragile topology beyond symmetry indicators, Phys. Rev. B **102**, 115135 (2020).
[20] B. Jiang, A. Bouhon, Z.-K. Lin, X. Zhou, B. Hou, F. Li, R.-J. Slager, and J.-H. Jiang, Experimental observation of non-Abelian topological acoustic semimetals and their phase transitions, Nat. Phys. **17**, 1239 (2021).
[21] Q. Guo, T. Jiang, R.-Y. Zhang, L. Zhang, Z.-Q. Zhang, B. Yang, S. Zhang, and C. T. Chan, Experimental observation of non-Abelian topological charges and edge states, Nature (London) **594**, 195 (2021).
[22] Q. Wu, A. A. Soluyanov, and T. Bzdušek, Non-Abelian band topology in noninteracting metals, Science **365**, 1273 (2019).
[23] F. N. Ünal, A. Bouhon, and R.-J. Slager, Topological Euler class as a dynamical observable in optical lattices, Phys. Rev. Lett. **125**, 053601 (2020).
[24] W. Zhao, Y.-B. Yang, Y. Jiang, Z. Mao, W. Guo, L. Qiu, G. Wang, L. Yao, L. He, Z. Zhou, Y. Xu, and L. Duan, Quantum simulation for topological Euler insulators, Commun. Phys. **5**, 223 (2022).
[25] W. J. Jankowski, A. S. Morris, A. Bouhon, F. N. Ünal, and R.-J. Slager, Optical manifestations of topological Euler class in electronic materials, arXiv:2311.07545.
[26] A. Avdoshkin and F. K. Popov, Extrinsic geometry of quantum states, Phys. Rev. B **107**, 245136 (2023).
[27] S. Kwon and B.-J. Yang, Quantum geometric bound and ideal condition for Euler band topology, Phys. Rev. B **109**, L161111 (2024).
[28] A. Bouhon, A. Timmel, and R.-J. Slager, Quantum geometry beyond projective single bands, arXiv:2303.02180.
[29] R.-J. Slager, A. Bouhon, and F. N. Ünal, Non-Abelian Floquet braiding and anomalous Dirac string phase in periodically driven systems, Nat. Commun. **15**, 1144 (2024).
[30] D. Vanderbilt, *Berry Phases in Electronic Structure Theory* (Cambridge University Press, Cambridge, England, 2018), 10.1017/9781316662205.
[31] N. R. Cooper, J. Dalibard, and I. B. Spielman, Topological bands for ultracold atoms, Rev. Mod. Phys. **91**, 015005 (2019).
[32] L. Duca, T. Li, M. Reitter, I. Bloch, M. Schleier-Smith, and U. Schneider, An Aharonov-Bohm interferometer for determining Bloch band topology, Science **347**, 288 (2015).
[33] M. Tarnowski, M. Nuske, N. Fläschner, B. Rem, D. Vogel, L. Freystatzky, K. Sengstock, L. Mathey, and C. Weitenberg, Observation of topological Bloch-state defects and their merging transition, Phys. Rev. Lett. **118**, 240403 (2017).
[34] C. D. Brown, S.-W. Chang, M. N. Schwarz, T.-H. Leung, V. Kozii, A. Avdoshkin, J. E. Moore, and D. Stamper-Kurn, Direct geometric probe of singularities in band structure, Science **377**, 1319 (2022).
[35] L. Tarruell, D. Greif, T. Uehlinger, G. Jotzu, and T. Esslinger, Creating, moving and merging Dirac points with a Fermi gas in a tunable honeycomb lattice, Nature (London) **483**, 302 (2012).
[36] F. Mahmood, C.-K. Chan, Z. Alpichshev, D. Gardner, Y. Lee, P. A. Lee, and N. Gedik, Selective scattering between Floquet-Bloch and Volkov states in a topological insulator, Nat. Phys. **12**, 306 (2016).
[37] Resulting in the π-Berry flux of a Dirac cone.
[38] Q. Wu, A. A. Soluyanov, and T. Bzdušek, Non-Abelian band topology in noninteracting metals, Science **365**, 1273 (2019).
[39] A. J. Beekman, J. Nissinen, K. Wu, K. Liu, R.-J. Slager, Z. Nussinov, V. Cvetkovic, and J. Zaanen, Dual gauge field theory of quantum liquid crystals in two dimensions, Phys. Rep. **683**, 1 (2017).
[40] B. Peng, A. Bouhon, B. Monserrat, and R.-J. Slager, Phonons as a platform for non-Abelian braiding and its manifestation in layered silicates, Nat. Commun. **13**, 423 (2022).
[41] S. Chen, A. Bouhon, R.-J. Slager, and B. Monserrat, Non-Abelian braiding of Weyl nodes via symmetry-constrained phase transitions, Phys. Rev. B **105**, L081117 (2022).
[42] See Supplemental Material at http://link.aps.org/supplemental/10.1103/PhysRevLett.133.093404 for more details: Sec. I, Frame charges and Dirac strings; Sec. II, moving through the BZ under a force and nonadiabatically through a node, including effects of experimental imperfections; Sec. III, method 1 and detailed accounting of dynamic phases; Sec. IV, Method 2; and Sec. V, Further numerical calculations and examples in Kagome lattice with next-nearest-neighbor tunneling terms and anomalous Euler phases under periodic driving, which includes Refs. [43–50].
[43] B. Peng, A. Bouhon, R.-J. Slager, and B. Monserrat, Multigap topology and non-Abelian braiding of phonons from first principles, Phys. Rev. B **105**, 085115 (2022).
[44] Y. D. Chong, Berry's phase and the anomalous velocity of Bloch wave packets, Phys. Rev. B **81**, 052303 (2010).

[45] P. Virtanen *et al.* (SCIPY1.0 Contributors), SCIPY1.0: Fundamental algorithms for scientific computing in Python, Nat. Methods **17**, 261 (2020).
[46] M. Tarnowski, F. N. Ünal, N. Fläschner, B. S. Rem, A. Eckardt, K. Sengstock, and C. Weitenberg, Measuring topology from dynamics by obtaining the Chern number from a linking number, Nat. Commun. **10**, 1728 (2019).
[47] C. Wang, P. Zhang, X. Chen, J. Yu, and H. Zhai, Scheme to measure the topological number of a Chern insulator from quench dynamics, Phys. Rev. Lett. **118**, 185701 (2017).
[48] F. N. Ünal, A. Eckardt, and R.-J. Slager, Hopf characterization of two-dimensional Floquet topological insulators, Phys. Rev. Res. **1**, 022003(R) (2019).
[49] F. N. Ünal, B. Seradjeh, and A. Eckardt, How to directly measure Floquet topological invariants in optical lattices, Phys. Rev. Lett. **122**, 253601 (2019).
[50] K. Wintersperger, C. Braun, F. N. Ünal, A. Eckardt, M. D. Liberto, N. Goldman, I. Bloch, and M. Aidelsburger, Realization of an anomalous Floquet topological system with ultracold atoms, Nat. Phys. **16**, 1058 (2020).
[51] The frame-charge assignment to each gap is a gauge choice, where only the relative sign in a gap is physically meaningful and the corresponding Euler class is gauge invariant.
[52] In general, ϕ^{frame} can be a generic function of ϕ^{path} but always winds by π as the latter winds by 2π. See Ref. [42] for more details and examples.
[53] We consider these interferometry angles to be such that the magnitude of frame rotation angle is the same on both paths, which can be controlled, e.g., using the techniques in Ref. [34] even for reduced lattice symmetries [42].
[54] M. Greiner, I. Bloch, O. Mandel, T. W. Hänsch, and T. Esslinger, Exploring phase coherence in a 2D lattice of Bose-Einstein condensates, Phys. Rev. Lett. **87**, 160405 (2001).
[55] Equivalently, the Dirac string can be deformed past the node along path I and omitted.
[56] Any relative dynamic phase appearing along the pre or postnode sections are irrelevant since they will not affect the populations.